Fracture Mechanics of Concrete and Concrete Structures - Assessment, Durability, Monitoring and Retrofitting of Concrete Structures- B. H. Oh, et al. (eds)

Numerical modeling of cracking of concrete due to corrosion of reinforcement – Impact of cover thickness and concrete toughness

A.O.S. Solgaard
COWI A/S, Kgs. Lyngby, Denmark and Department of Civil Engineering, Technical University of Denmark (DTU),Kgs. Lyngby, Denmark

A. Michel, H. Stang, & M. R. Geiker
Department of Civil Engineering, Technical University of Denmark (DTU),Kgs. Lyngby, Denmark

C. Edvardsen & A. Küter
COWI A/S, Kgs. Lyngby, Denmark

ABSTRACT: Deterioration of reinforced concrete structural members is an increasing problem in the construction sector. The formation of corrosion products from steel reinforcing bars (rebars) leads to an increase in volume and the possibility of cracking and spalling of the concrete as the tensile capacity of the concrete matrix is exceeded. The ongoing work concerns a parametric study of cracking of cover concrete due to reinforcement corrosion. The basis of the simulations is a numerical fracture mechanical model for crack initiation and propagation in concrete covers. The fracture mechanical model is based on the theory of the fictitious crack, where the expansion of the corrosion products is modeled by the use of a fictitious thermal load. The aim of the paper is to investigate the influence of the cover thickness and the ductility of the concrete on the crack initiation and crack propagation due to reinforcement corrosion. The paper contributes to the understanding of cover cracking due to reinforcement corrosion with numerical investigations of the mechanical parameters influencing the crack initiation and propagation.

1 INTRODUCTION

Corrosion of reinforcement embedded in concrete is one of the main deterioration processes of reinforced concrete structures and has been the pivot of numerous projects. As the corrosion products take up more volume than the original steel consumed, a pressure is build up in the interface between reinforcement and concrete. The increase in pressure eventually leads to cracking of the concrete cover. This allows for faster ingress of de-passivating substances, e.g. Cl ions and CO_2, leading to faster deterioration of the reinforcement.

Cracking of concrete due to reinforcement corrosion has been investigated experimentally and analytically in a number of papers. The experimental work mainly concerns accelerated tests where a current is applied to the reinforcement to control the rate of corrosion e.g. Andrade et al. (1993) and Alonso et al. (1998). The models for corrosion induced cracking of concrete concerns the time to corrosion induced cracking e.g. Liu & Weyers (1998), modeling of cracking assuming smeared cracking, e.g. Molina et al. (1993), modeling of cracking assuming an inner softening band, Noghaibi (1998) and analytical models based on the theory of a thick-walled cylinder, Chernin et al. (2009). In parts of the literature experimental results are used for verification of the presented models. However, there seems to be an in-consistency between proposed model and experimental data. This has resulted in the assumption of a porous zone around the reinforcement, where the corrosion products diffuse into without increasing the pressure in the interface.

The scope of the present paper is to analyze crack initiation and propagation in concrete due to reinforcement corrosion by the use of a numerical fracture mechanical model based on the effective cohesive relationship of the concrete. The relationship between the thickness of the concrete cover and the diameter of the reinforcement and crack initiation and propagation is investigated for increasing thicknesses of corrosion products. Furthermore the initiation and extent of crack propagation is modeled for plain concrete (PC) and fibre reinforced concrete (FRC) in order to investigate the impact of the increased ductility of FRC. The latter is of great interest, as small crack openings do not seem to have an effect on the ingress of ions and CO_2 leading to increased corrosion of embedded reinforcement.

As mentioned earlier cracking of cover concrete has been investigated in numerous research projects, experimentally as well as analytically. However, simulations concerning the influence of the ductility of the concrete cover due to e.g. addition of fibres have, to the knowledge of the author, not been investigated thoroughly. Hence the present paper contributes to these investigations with a modeling approach for cracking of covers due to reinforcement corrosion.

2 THEORY

2.1 *Corrosion of reinforcement*

Corrosion of reinforcement embedded in concrete is a process influenced by numerous independent factors. Depending on the environmental conditions, different corrosion processes can take place. Analyses of concrete cover cracking due to corrosion of reinforcement under laboratory conditions have been performed in numerous research projects, e.g. Val et al. (2009), Isgor & Razaqpur (2006) and Caré et al. (2008). However, there is a discrepancy between the different research projects which corrosion products to take into account. In the present context only the formation of $Fe_2O_3 \cdot H_2O$ is taken into account. Formation of other products with other expansion coefficients is beyond the scope of the present work. The corrosion is assumed uniform, and a sketch of the reinforcement is given in Figure 1.

Diffusion of corrosion products into the concrete matrix is not taken into account in the present model. Hence the volume of corrosion products leading to an increase in the pressure in the interface is proportional to the volume of consumed steel.

$$\Delta V_c = \eta_{\mathrm{vol}} \Delta V_s \tag{1}$$

where ΔV_c is the volume of corrosion products, ΔV_s is the volume of consumed steel and η_{vol} is the volume expansion coefficient of the corrosion products.

Assuming uniform corrosion, the depth of consumed steel due to corrosion can be determined from Faraday's law, cf. Equation 2:

$$X(t) = \frac{M}{\rho n F} \int_0^t i_{cor}(t) dt \tag{2}$$

where M is the atomic mass of iron, ρ is the density of iron, n is the valence of iron, F is Faraday's number, t is the time and i_{cor} is the corrosion current density.

As the thickness of the corrosion products is very small compared to the radius of the reinforcement, we get:

$$t_{cor} = \eta_{lin} X(t) \tag{3}$$

where t_{cor} is the thickness of the corrosion products and η_{lin} is the linear expansion coefficient of the corrosion products. The linear expansion coefficient for an isotropic material is 1/3 of the volume expansion coefficient. It is seen that the thickness of the corrosion products t_{cor} can be linked to time via Equations 2-3.

2.2 *Description of model*

The expansion of the corrosion products is modeled by the use of a fictitious thermal load. The approach has earlier been used by e.g. Molina et al. (1993). The modeling approach used in the present context is described in the following.

1) The rebar with initial radius is modeled, cf. Figure 1 for $t=t_0$.

2) A prescribed thickness of consumed steel, X(t), is applied to the model, cf. Figure 1 for $t=t_{1,1}$. The original rebar is now transformed into two domains with different material properties: An inner core of steel with Young's modulus E_{st} and Poisson's ratio γ_{st} and an outer perimeter of corrosion products with mechanical properties Young's modulus E_{cor} and Poisson's ratio γ_{cor}.

3) A thermal load, T_{cor}, corresponding to the linear expansion coefficient of corrosion products is applied to the outer perimeter of the rebar. The thermal load of the outer perimeter causes an increase in the volume of the corrosion products, cf. Figure 1 for $t=t_{1,2}$.

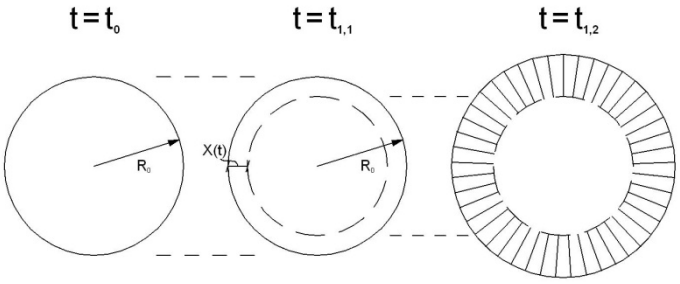

Figure 1. Schematic illustration of modeling the expansion of corrosion products.

Please note that $t_1 > t_0$ and that the modeling is divided in two steps for $t=t_1$ viz. $t_{1,1}$ and $t_{1,2}$. Furthermore, the free expansion of the corrosion products, as shown to the right of Figure 1 does not take place when the rebar is embedded in the concrete body.

As the thickness of the corroded steel, X(t), has to be prescribed prior to modeling it is not possible to use the model for transient modeling of the crack propagation due to an increase in corrosion products. Thus in order to obtain the crack initiation and propagation over time, meaning for an increase in X(t), cf. Equation 2 it is necessary to run a series of analyses for different X(t).

The variation in mechanical properties and temperature through the cross-section for $t=t_1$ is sketched in Figure 2:

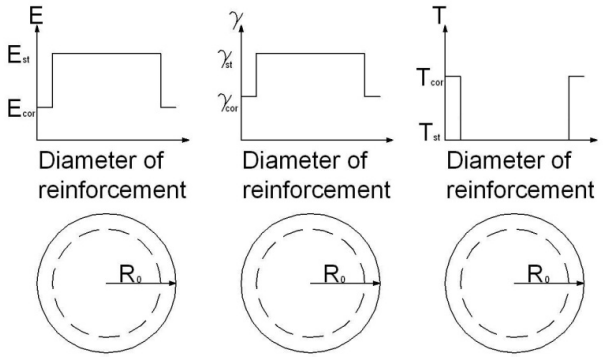

Figure 2. Schematic illustration of the distribution of mechanical properties and temperature across rebar cross section for $t=t_1$.

Please note that in Figure 2, the variations of mechanical properties are not in scale. The thermal load applied to the perimeter of the rebar $T_{cor}=2.1$.

The interaction between the reinforcement and the confining concrete is shown in Figure 3.

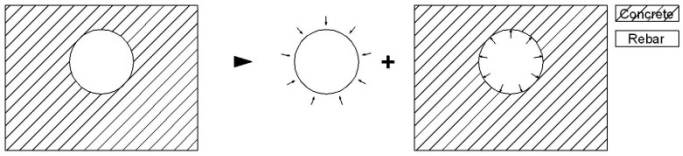

Figure 3. Schematic illustration of pressure on confining concrete due to expansive corrosion products. Adapted from Liu & Weyers (1998).

From Figure 3 it is seen that the increase of volume due to corrosion causes pressure in the steel-concrete interface and this pressure must be counteracted by the confining concrete.

2.3 *Fracture mechanics of concrete*

The crack initiation and propagation in a semi-infinite concrete body has been modeled in the commercial FE-program DIANA by the use of a discrete crack formulation based on the fictitious crack model suggested by Hillerborg et al. (1976). The cross section of the model used is shown in Figure 4.

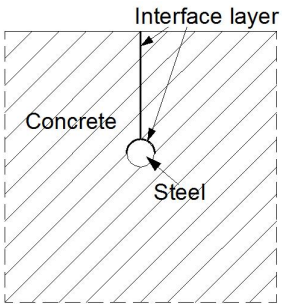

Figure 4. Cross section of model used for determination of crack initiation and crack propagation.

The elements outside the crack are considered to behave linear elastically and isotropically, whereas the elements in the interface are behaving non-linear according to a predefined cohesive law giving the relationship between stress and crack opening. A total of app. 900 elements each with 16 degrees of freedom have been used for the mesh.

In the modeling approach used for the crack initiation and propagation it is assumed that:

$$\sigma = \begin{cases} \sigma_e(\varepsilon) = E_c\varepsilon & \textit{precracked state} \\ \sigma_w(w) = g(w)f_t & \textit{cracked state} \end{cases} \quad (4)$$

where σ_e is the stress in the elastic domain, E_c is Youngs modulus for concrete, ε is the elastic strain, σ_w is the bridging stress across the crack, g(w) is the dimensionless softening function and f_t is the tensile strength of concrete. The cohesive laws used in the present context are described in detail in the model description.

The interface layer is placed right above the reinforcement through the cover concrete. Experimental investigations of cracking of concrete due to reinforcement corrosion, e.g. Liu & Weyers (1998), have showed that cracks are mainly formed vertically above the reinforcement through the cover layer. Thus the position of the pre-defined crack path, the interface layer, is in accordance with experimental observations. The mesh used for the modeling is shown in Figure 5:

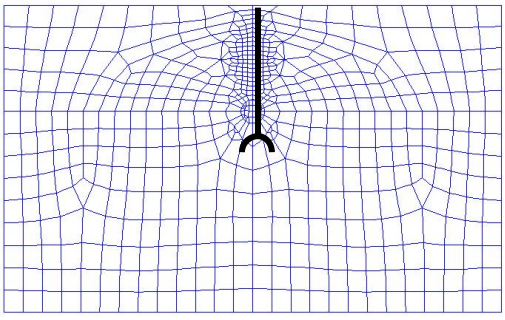

Figure 5. Mesh for modeling the cracking of cover due to reinforcement corrosion.

The bold lines indicate the position of the interface layer. It is seen from Figure 5, that the meshing is denser at the interface layer. The meshing for the reinforcement and the interface layer is shown in Figure 6:

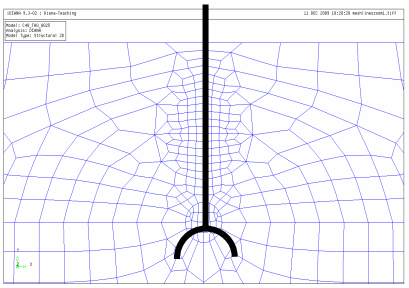

Figure 6. Meshing of reinforcement and interface layer.

The measures of the semi-infinite concrete body are 100 mm on each side of the reinforcement, except from cover, which has revealed to be sufficient to ensure that the behavior of the body is semi-infinite. Modeling is conducted for plain strain and cracking is solely modeled as Mode-I, opening mode, cracking.

A slip interface has been modeled around the upper half of the rebar. The interface elements are used for simulation of the debonding in the steel-concrete interface and have Mixed-Mode properties and a shear retention factor of app. 3.

Further descriptions of the model are given in Michel et al. (2009).

3 MODELING OF CRACKING

The crack initiation and propagation in reinforced concrete due to reinforcement corrosion is modeled for various cover thicknesses and various mechanical properties of the cover layer, viz. cohesive relationships.

3.1 *Parameters for the model*

In order to describe the influence of the cover layer on the cracking, different values for the thickness of the cover layer have been investigated, viz. 10, 20 and 40 mm. For all of the simulations, the diameter of the reinforcement bar is constant. The values for the mechanical properties of the reinforcement, the elastic domain of concrete and corrosion products are constant for all of the simulations and given in Table 1:

Table 1. Constants for fracture mechanical model.

Parameter	Value	Dimension
Young's modulus for steel	210	GPa
Young's modulus for concrete	31	GPa
Young's modulus for corr. product	2.1	GPa
Tensile strength of concrete	3.0	MPa
Poisson ratio of steel	0.3	-
Poisson ratio of concrete	0.2	-
Poisson ratio of corr. products	0.2	-
Expansion coef. of corr. product	2.1	m/K^{-1}
Diameter of reinforcement	10	mm

In order to investigate crack initiation and propagation for different mechanical properties of concrete the cohesive relationships for plain concrete and fibre reinforced concrete are investigated.

For the modeling of the cohesive relationship, a bi-linear model has been suggested. For plain concrete the cohesive relationship does not vary significantly. However, according to Löfgren et al. (2008), the addition of fibres to the matrix changes the stress-crack opening relationship.

According to Hillerborg et al. (1976), the toughness of concrete should be determined from the fracture energy, the elastic modulus and the tensile strength:

$$l_{ch} = \frac{E_c G_f}{f_t^2} \tag{5}$$

where l_{ch} is the characteristic length of the material, E_c is the elastic modulus of concrete, G_f is the fracture energy and f_t is the tensile strength. Note that the characteristic length is inverse proportional to the tensile strength squared. Thus high strength materials, which are usually brittle will get a lower characteristic length than low strength materials with the same elastic modulus and fracture energy Rosello et al. (2005).

Two different approaches for the mechanical properties of the cover layer have been used:

1) The slope of the second branch, a_2, is constant and the intersection of the second branch with the ordinate-axis, b_2, is shifted in equal intervals. The cohesive parameters are given in Table 2.
2) The slope of the second branch, a_2, is halved between the different approaches and the intersection of the second branch with the ordinate axis, b_2, is shifted in equal intervals. The cohesive parameters are given in Table 3.

In the following, the cohesive relationships modeled from approach 1 are named $b_{2,1}$-$b_{2,4}$, and the relationships obtained from approach 2 are named $a_{2,1}$-$a_{2,4}$.

Table 2. Material parameters for modeling approach 1.

	$b_{2,1}$	$b_{2,2}$	$b_{2,3}$	$b_{2,4}$
a_1 [mm^{-1}]	27.5	19.2	10.8	2.5
a_2 [mm^{-1}]	2.5	2.5	2.5	-
b_2 [-]	0.5	0.67	0.83	1
G_f [J/m^2]	165	277	421	600
l_{ch} [mm]	568	954	1450	2067

Table 3. Material parameters for modeling approach 2.

	$a_{2,1}$	$a_{2,2}$	$a_{2,3}$	$a_{2,4}$
a_1 [mm^{-1}]	27.5	19.2	110	0.3
a_2 [mm^{-1}]	2.5	1.2	0.6	-
b_2 [-]	0.5	0.67	0.83	1
G_f [J/m^2]	165	543	1685	4800
l_{ch} [mm]	568	1870	5804	16533

Note that the cohesive relationships $b_{2,1}$ and $a_{2,1}$ equals as these are the relationships forming the basis of the other relationships. These relationships reflect the mechanical properties of plain concrete.
The cohesive relationships are illustrated in Figures 7-8:

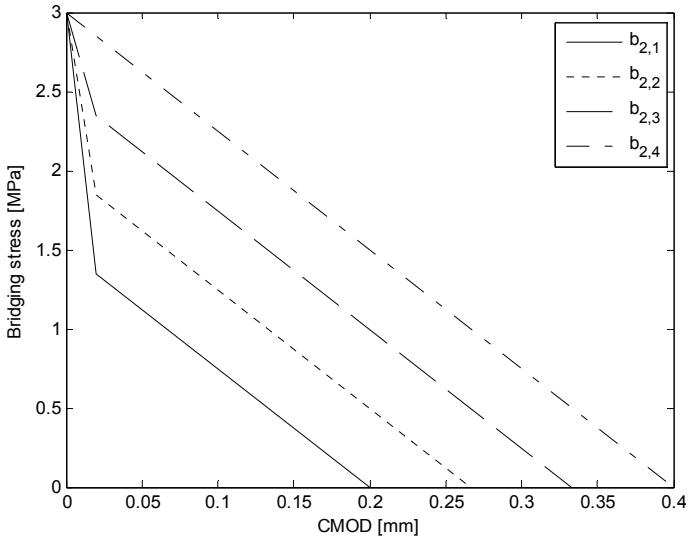

Figure 7. Cohesive laws for approaches $b_{2,1}$-$b_{2,4}$.

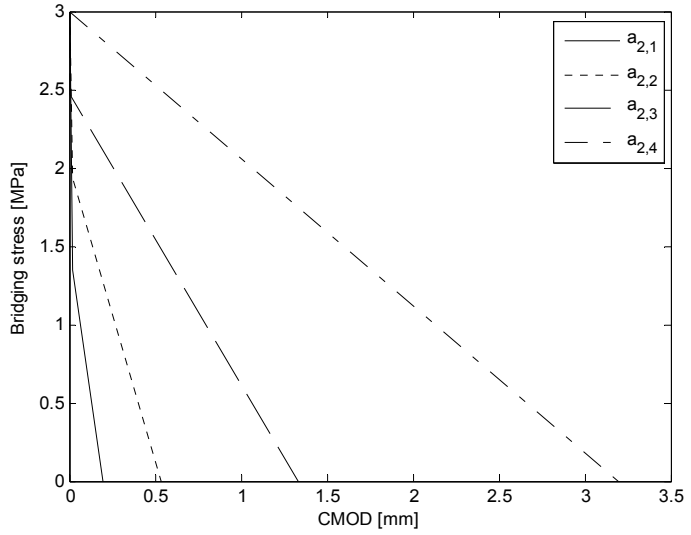

Figure 8. Cohesive laws for approaches $a_{2,1}$-$a_{2,4}$.

Thus in total seven different cohesive relationships are investigated. Note the difference in the ordinate axis for Figures 7 and 8. According to Kazemi et al. (2007), the fracture energy is increased app. 11 times when small amounts (0.5 vol-%-1.5 vol-%) of 32mm steel fibres are added to plain concrete.

3.2 *Limitations for modeling approach*

The crack initiation and crack propagation in reinforced concrete described in the present paper is modeled by the use of a fracture mechanical model, where a fictitious thermal load is applied to the reinforcement in order to simulate the expansive corrosion products. This modeling approach has also been used by e.g. Molina et al. (1993).

Once the crack is initiated and starts to propagate it is assumed that the corrosion products do not intrude into the crack. Furthermore the porous ITZ around the reinforcement is not taken into account, thus it is assumed that the corrosion products do not diffuse into the ITZ but contributes to the increase in pressure in the interface between reinforcement and concrete. Thus the presented model represents a conservative simulation of the buildup of pressure due to corrosion of reinforcement.

Due to limitations in the FE-modeling software the minimum thickness of the consumed steel, X(t) cf. Figure 1 is 2.5μm. Consequently the crack initiation cannot be simulated for small cover thicknesses with the present model.

3.3 *Results from modeling*

The modeling has been conducted for small crack openings at the surface. Thus the thickness of the corrosion products is varied between app. 5μm and 21μm. Thus it is not possible to investigate the crack initiation for small cover thicknesses (10mm and 20mm). In order to investigate the crack propagation through the concrete cover the crack opening at the steel surface, 1.5 mm above the steel surface and at the concrete surface have been calculated for all geometries and cohesive relationships.

3.3.1 *Crack initiation and propagation*

The crack initiation and propagation at different locations through the cross section for 10mm and 40mm cover thickness for plain concrete, approach $b_{2,1}$, are shown in Figures 9-10:

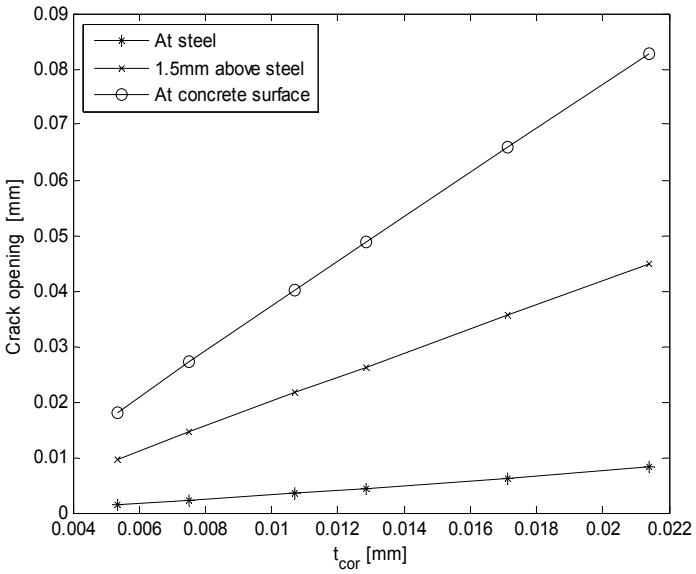

Figure 9. Results from modeling of crack initiation and propagation in plain concrete, $b_{2,1}$, for C=10mm.

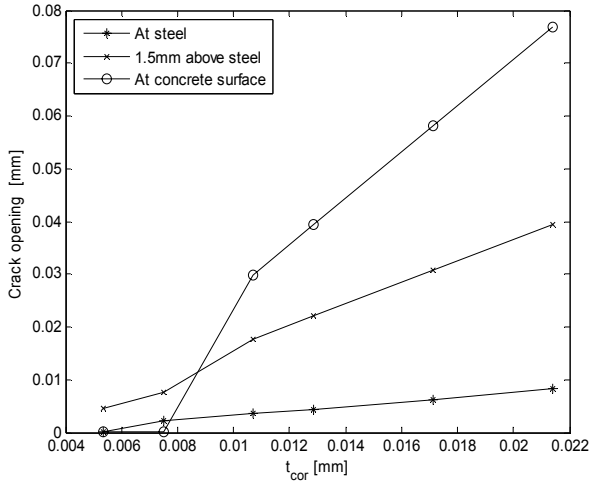

Figure 10. Results from modeling of crack initiation and propagation in plain concrete, $b_{2,1}$, for C=40mm.

3.3.2 *Influence of cohesive relationship on cracking*

In order to illustrate the influence of the cohesive relationship on the cracking of the cover layer, the displacements at different locations for the cohesive relationships for plain concrete, $b_{2,1}$, and the most ductile FRC investigated, $a_{2,4}$, for C=10mm and C=40mm are illustrated in Figures 11-12:

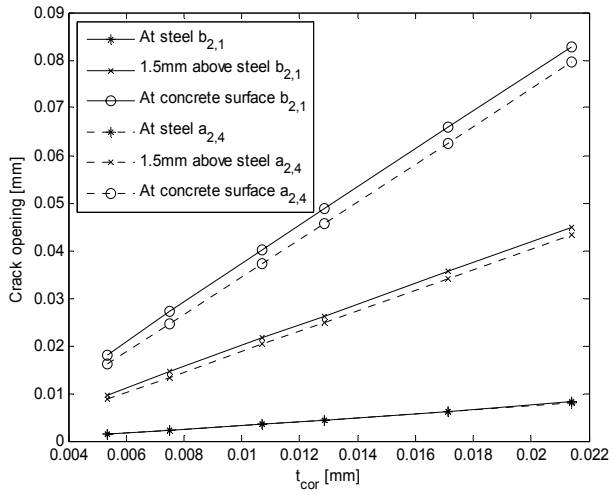

Figure 11. Results from modeling of crack initiation and propagation in plain concrete and FRC for C=10mm.

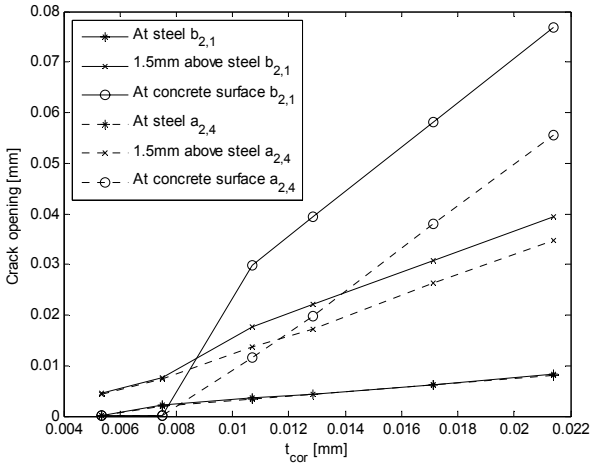

Figure 12. Results from modeling of crack initiation and propagation in plain concrete and FRC for C=40mm.

3.3.3 *Analyzes of CMOD and cover thickness*

In order to evaluate the influence of the ductility of the cover concrete on the crack initiation and propagation, the crack opening at the concrete surface and at the concrete-steel interface have been plotted for various cover thicknesses and various material parameters in Figures 13-14.

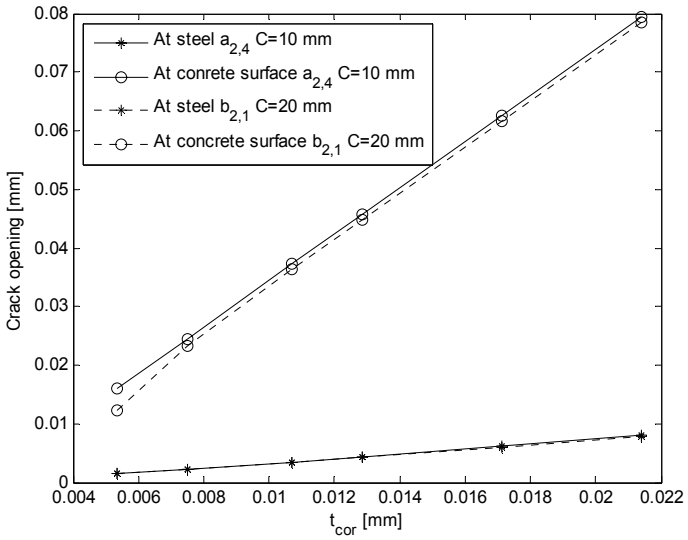

Figure 13. Crack opening at concrete surface and at steel-concrete interface for C=20mm and $b_{2,1}$ vs. C=10mm and $a_{2,4}$.

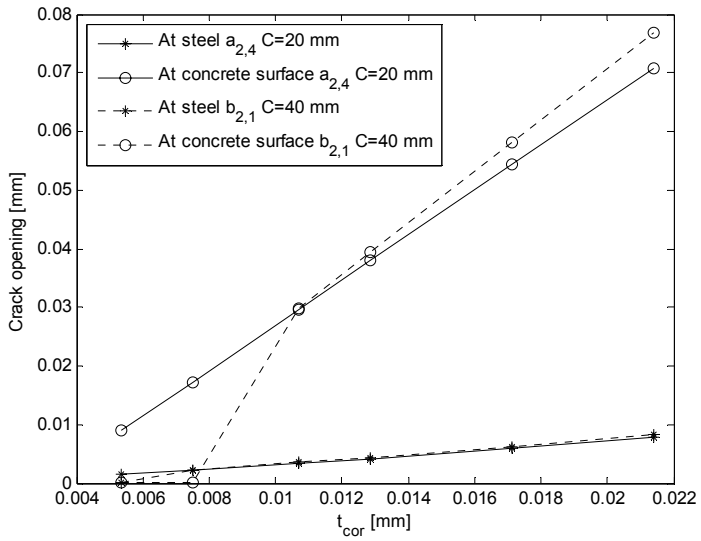

Figure 14. Crack opening at concrete surface and at steel-concrete interface for C=40mm and $b_{2,1}$ vs. C=20mm and $a_{2,4}$.

3.3.4 *Analyzes of the two approaches for modeling the cohesive relationship*

The cohesive relationships investigated in the present paper are modeled from two different approaches cf. Section 3.1. Thus the difference between the two approaches is investigated by analyzing the crack opening at the concrete surface for cover thicknesses 10mm and 40mm. The results are shown in Figures 15-16:

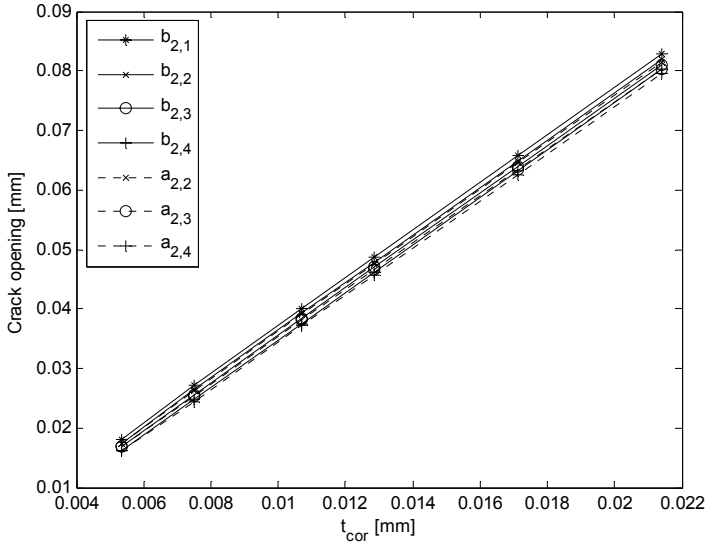

Figure 15. Crack opening at concrete surface for C=10mm and various approaches for the cohesive relationship.

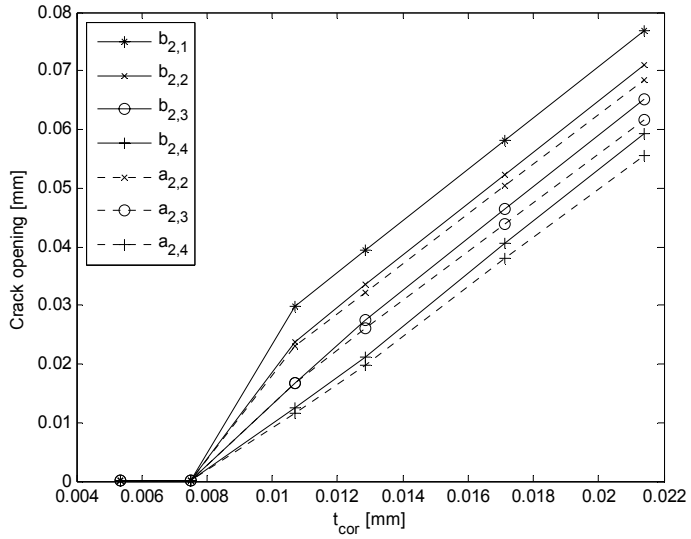

Figure 16. Crack opening at concrete surface for C=40mm and various approaches for the cohesive relationship.

4 DISCUSSION

Concerning the cohesive relationships used for the simulations it is seen, that the variation mainly concerns the second branch of the cohesive relationship. The first branch of the cohesive relationship concerns the concrete matrix, whereas the second branch concerns the amount of fibres, properties of the fibres etc. Löfgren et al. (2008). Thus the variations of the cohesive relationship given in Tables 1-2 concern variation of the second branch in order to investigate the properties changed when fibres are added. Comparing the ductility of the assumed cohesive relationships, Tables 1-2, with values from the literature, Kazemi et al (2007), it is seen, that these reflects the properties of concrete with small amounts of fibres (0.5 vol-% - 1.5 vol-%).

From Figure 9 it is seen, that when a certain value of the corrosion thickness is reached, the crack opens linearly with the increase in the corrosion thickness. Comparing Figure 9 and 10 it is seen, that an increase in the cover thickness, requires a larger corrosion thickness to initiate a crack. Additionally it is seen from Figures 9-10 that the crack propagation changes significantly when the cover is increased from 10mm to 40mm. For the values of t_{cor} simulated in the present context, the crack propagation for C=40mm is stable inside the concrete cover and propagates until it reaches the concrete surface. This is not the case for C=10mm where the crack propagates to the surface for very small values of t_{cor} (< 5μm).

Regarding the effect of the mechanical properties of the concrete on the crack initiation and propagation, it is seen from Figure 11 that the crack opening at the steel-concrete interface is regardless of the cohesive relationship for materials with the same tensile strength. Considering the crack opening at the surface of the concrete, which is a governing parameter when discussing cracking of concrete, it is seen from Figure 11, that the crack opening is decreased app. 28% for the same t_{cor} comparing plain concrete with fibre reinforced concrete for C=10mm. Moreover, it is seen that in order to reach the same crack opening at the concrete surface, the thickness of corrosion products has to be increased by app. 33% when comparing plain concrete with fibre reinforced concrete. The thickness of the corrosion products can be linked to time from numerical modeling concerning evolution of a corrosion cell, e.g. the model proposed by Michel et al. (2009) and Equations 2-3.

The effect of the increased ductility of the material, when adding fibres, is more pronounced when the cover thickness is increased to e.g. 40mm, cf. Figure 12. When the crack is opening the thickness of the corrosion products has to be app. 50% higher for fibre reinforced concrete, approach $a_{2,4}$, than for plain concrete, approach $b_{2,1}$, in order to obtain the same crack opening at the concrete surface.

From Figure 13 it is seen that the mechanical performance of a 10mm cover of FRC with cohesive parameters as material $a_{2,4}$ is very similar to the mechanical performance of a 20mm cover of plain concrete with mechanical properties as material $b_{2,1}$. Finally, from Figure 14 it is seen that the same mechanical effect can be obtained by applying 20 mm FRC ($a_{2,4}$) instead of 40 mm plain concrete ($b_{2,1}$).

The influence of constructing the cohesive relationship from two different approaches, cf. Section 3.1, is illustrated in Figures 15-16. It is seen that the influence on the crack opening at the concrete surface from the different cohesive relationships is increased with the increase in cover thickness.

Though the same mechanical properties of the cover can be obtained for smaller covers with FRC

than larger covers of plain concrete it is noted, that changing the cover thickness influences the transport of hazardous substances to the reinforcement. Thus the initiation of corrosion might be advanced when the cover is decreased. However in order to evaluate this issue, a simulation of the formation of corrosion cells on embedded rebars has to be performed, e.g. like proposed by Michel et al. (2009).

5 CONCLUSION

A numerical model for the initiation and propagation of cracks in a semi-infinite concrete body has been presented. The model is based on Hillerborgs fictitious crack model where MODE I cracking and Mixed mode cracking is taken into account. The cracking of the cover is modeled by the use of interface elements with a cohesive relationship and the expansion of the corrosion products is modeled with a fictitious thermal load. A uniform distribution of the corrosion products is assumed.

Based on the numerical simulation of the crack initiation and propagation in concrete covers due to reinforcement corrosion it is concluded:

- For the cohesive relationships investigated, the crack opening at the steel-concrete interface is independent of the ductility of matrix.
- After a certain thickness of the corrosion products is reached, the crack propagation is app. linear with t_{cor}.
- The crack opening at the concrete surface is almost independent of the mechanical properties of the matrix when regarding a small cover (10mm). However, as the cover thickness is increased the influence of the material properties gets more pronounced, and increased ductility of the material leads to decreased crack opening at the concrete surface. Furthermore the crack propagates to the concrete surface for small covers (C=10mm) and small values of t_{cor} whereas the crack propagation is stable inside the concrete cover for larger cover thicknesses (C=40mm).
- The mechanical performance of a 20mm cover of plain concrete, $b_{2,1}$, is within the same range as the mechanical performance of FRC, $a_{2,4}$. The same can be seen for 40mm plain concrete, $b_{2,1}$, and 20mm FRC, $a_{2,4}$.

ACKNOWLEDGEMENTS

The first author is grateful to COWI A/S and The Danish Agency for Science, Technology and Innovation for the full support of the PhD project "Application of Fibre Reinforced Concrete in Civil Infrastructure" for Anders Ole Stubbe Solgaard.

REFERENCES

Andrade, C. et al. 1993. Cover cracking as a function of bar corrosion: Part I- Experimental test. *Materials and Structures*, 26:453-464.

Alonso, C. et al. 1997. Factors controlling cracking of concrete affected by reinforcement corrosion, *Materials and Structures,* 31: 435-441.

Caré, S., Nguyen, Q. T., L´Hostis, V. & Berthaud, B. 2008. Mechanical properties of the rust layer induced by impressed current method in reinforced mortar. *Cement and Concrete Research* 38: 1079-1091.

Chernin, L. et al. 2009. Analytical modelling of concrete cover cracking caused by corrosion of reinforcement. *Materials and Structures* published online

Hillerborg, A. et al 1976. Analysis of crack formation and crack growth in concrete by means of fracture mechanics and finite elements. *Cement and Concrete Research*, 6: 773-782.

Isgor, B. O. & Razaqpur, G. A. 2006. Modelling steel corrosion in concrete structures. *Materials and Structures* 39: 291–302.

Kazemi, M. T., et al. 2007, Cohesive Crack Model and Fracture Energy of Steel-Fiber-Reinforced-Concrete Notched Cylindrical Specimens, *Journals of Materials in Civil Engineering* 19(10): 884-890.

Liu, Y. & Weyers, R.E. 1998. Modeling the Time-to-Corrosion Cracking in Chloride Contaminated Reinforced Concrete Structures, *ACI Materials Journal* 95(6): 675-681.

Löfgren, I., et al. 2008. The WST method, a fracture mechanics test method for FRC, *Materials and Structures,* 47: 197-211.

Michel, A., et al. 2009 Modeling Formation of Cracks in Concrete Cover due to Reinforcement Corrosion, *FraMCos-7 - 7th International Conference on Fracture Mechanics of Concrete and Concrete Structures; Conference proceedings. Jeju, Korea, 23-28 May 2010.*

Molina, F.J. et al. 1993. Cover cracking as a function of rebar corrosion: Part 2 – Numerical model, *Materials and Structures,* 26:532-548.

Noghabai, K. 1999. FE_Modelling of cover splitting due to corrosion by use of inner softening band. *Materials and Structures,* 32: 486-491.

Rosello et. al 2005. Fracture of model concrete: 2. Fracture energy and characteristic length, *Cement and Concrete Research,* 36:1345-1353.

Val, D. V., Chernin, L. & Stewart, M. G. 2009. Experimental and numerical investigation of corrosion-induced cover cracking in reinforced concrete structures. *Journal of Structural Engineering* 135:376-385.